

A dual-band miniature uniplanar antenna on epoxy reinforced woven glass material for WiMAX, WLAN, UWB, and X-band applications

Md. M. Alam^a, R. Azim^{b,*}, N. M. Sobahi^a, A. I. Khan^c

^a*Department of Electrical and Computer Engineering, King Abdulaziz University, Jeddah 21589, Saudi Arabia*

^b*Department of Physics, University of Chittagong, Chattogram 4331, Bangladesh*

^c*Computer Science Department, King Abdulaziz University, Jeddah 21589, Saudi Arabia*

In this paper, a dual-band miniature uniplanar antenna is presented. The antenna size is 24.5 mm × 20 mm × 1.6 mm which consists of a modified bow-tie-shaped radiator, an inverted L-shaped ground plane, and an extended inverted U-shaped ground plane, and designed on the single side of a low-cost epoxy matrix reinforced woven glass material with permittivity 4.6. The numerical results confirm that the radiator is effectively coupled with the coplanar ground planes and the investigated antenna can cover dual frequency bands ranging from 3.32 to 10.9 GHz, and 11.88 to 17.77 GHz. The measured results of the prototype in frequency-domain and time-domain are obtained and compared with the simulated results. The results indicate that the proposed antenna demonstrates good performance over the dual impedance bands, which makes it a very potential candidate for WiMAX, WLAN, UWB, X-band, and Ku-band wireless communication applications.

(Received September 18, 2021; Accepted December 6, 2021)

Keywords: Epoxy-resin material, Antenna, Uniplanar, WiMAX; WLAN, UWB, X-band

1. Introduction

Recently ultra-wideband (UWB) and super-wide (SWB) technology emerged as an attractive solution for both fixed and portable wireless communication applications including WBAN, WLAN, WPAN, positioning, tracking, microwave imaging, GSM phone, satellite TV, etc. As UWB and SWB technology provides higher data rates and very large bandwidth, they can be used in both civil and military to transfer video, audio, and data at a higher speed [1 - 2]. As a key component, the designing of a miniature antenna with the attractive features of low complexity, low cost, high data transfer capacity, high immunity to multi-path interference, and operating over wide/ultra-wide/super-wide frequency band is a very challenging task [3]. The antenna must achieve sufficient working bandwidth to cover UWB including WiMAX, WiFi, WLAN as well as X- and Ku-bands. Moreover, it should be simple, planar, and less expensive.

Currently, UWB/SWB communication systems preferred planar antennas as they are small, low profile, lightweight, ease integration in portable devices, and can exhibit omnidirectional and directional radiation patterns. To meet UWB/SWB requirements, a good number of microstrip-fed planar antennas and coplanar waveguide (CPW)-fed antennas have been investigated [4 - 22]. For example, in [5], an elliptical dipole antenna is illustrated for UWB uses. To improve the bandwidth and gain, here, elliptical grooves are etched on the arms of the dipole and the antenna achieves a frequency band that varies from 2.7 to 11 GHz. However, the antenna possesses a relatively large size of 106 mm × 85 mm. For indoor wireless access, in [6] a circular polarized UWB antenna is presented. With a dimension of 75 mm × 75 mm, the designed antenna attained an impedance band ranging from 2.94 to 10.06 GHz. For wearable use, in [7], a flexible UWB antenna is reported. The designed antenna with a footprint of 80 mm × 67 mm is consists of

* Corresponding author: rezaulazim@cu.ac.bd

two modified arc-shaped radiators and a full ground plane and achieved an operating band of 3.7 to 10.3 GHz. In [8], a CPW-fed Mercedes-shaped monopole antenna is presented for UWB applications. The Mercedes-shaped radiator of the presented antenna consists of a three-legged lead embedded circular ring and is effectively coupled with two coplanar ground planes and achieved a simulated operating band of 2.1 to 12.6 GHz. A CPW-fed semicircular UWB antenna is presented in [9]. The designed antenna is consisting of a semicircular radiator with dual slots and two coplanar ground planes and can operate over the 3 to 18 GHz band. But it possesses a relatively large of $40 \text{ mm} \times 53.3 \text{ mm}$ and is not suitable for portable communication devices. In [10], a printed circular disc antenna is reported for UWB applications. The antenna is made up of a microstrip line-fed circular radiator and a partial ground plane and etched on both sides of a $42 \text{ mm} \times 50 \text{ mm}$ size FR4 substrate. The circular patch of the antenna matched well with the ground plane resulting in the attaining of a wide operating band of 2.78 - 9.78 GHz. For UWB applications, a coplanar strip-fed spiral antenna that achieved an operating band of 3.5 to 11 GHz is reported in [11]. But it possesses a larger volumetric size of $40 \text{ mm} \times 50 \text{ mm}$. In [12], a planar Vivaldi antenna is presented for UWB applications. Using a stepped connection structure, the designed antenna achieved an operating band of 3 to 15.1 GHz. However, due to the long-tapered slot, it occupies a relatively large area. For ultra-wideband operation, in [13], a $35 \text{ mm} \times 54 \text{ mm}$ size Fractal antenna is reported. In this design, Fractal geometry is adopted by iteration of square slots into the hexagonal radiator and the antenna achieved a bandwidth of 11.4 GHz. In [14], a horizontally polarized UWB antenna is presented. With a dimension of $57 \text{ mm} \times 32 \text{ mm}$, it achieved an impedance band ranging from 3.2 to 13.2 GHz. In [15], a triangular-shaped CPW-fed monopole antenna is presented. Connecting the two coplanar grounds with a top-cross-loop, the operating bandwidth and gain are improved. However, it occupies an area of 1650 mm^2 in FR4 substrate. In [16], a UWB antenna with an electrical size of $0.34\lambda \times 0.35\lambda$ is presented. The designed antenna is composed of an annular ring radiator and a partial ground plane and can cover the 2.6 to 12.3 GHz band. A wideband defected crown-shaped antenna is presented in [17]. Utilizing a bigger U-shaped radiator along with two coplanar ground planes, the designed antenna achieved an impedance band ranging from 4.5 - 13.5 GHz. In [18], a bird face-shaped monopole antenna is presented for UWB applications. With a dimension of $0.25\lambda \times 0.36\lambda$, the designed antenna achieved a working band of 3.1 to 12.3 GHz. In [19], a narrow slot UWB antenna that uses slot line CPW transition is reported. The designed antenna consisting of a slot line, a CPW transition line, and a four-way open slot and can operate over the 2.9 to 11.8 GHz band. In [20], an open slot UWB antenna is presented. Using symmetric open slots and a U-shaped feed line, this design excites at four resonant modes and can operate over the 3.15 to 10.55 GHz band. Though many of the reported antennas achieved wide/ultra-wide/super-wide operating bands, they possess either a large size, complex structure, or difficult to fabricate. Moreover, some of them do not cover the 12 - 18 GHz band for Ku-band communication applications.

This paper presents epoxy reinforced woven glass material based miniature planar antenna ($24.5 \times 20 \times 1.6 \text{ mm}^3$) with an electrical dimension of $0.27\lambda \times 0.22\lambda$ and dual operating bands of 3.32 - 10.9 GHz, and 11.88 - 17.77 GHz. The dual-band characteristics are obtained by two coplanar ground planes and an altered bow-tie-shaped radiator. The simulated results are compared with the measured results, which indicate that the studied antenna has a very excellent performance in the frequency domain as well as time-domain. Consequently, the proposed antenna is a good fit for a range of wireless communication services like WiMAX (3.5/5.8 GHz), WiFi/WLAN (3.6/4.9/5/5.9 GHz), radio-frequency systems (4.5 - 7.0 GHz, 13.4 - 14 GHz), ITU band communication (8.025 - 8.4 GHz), UWB communication systems (3.1 - 10.6 GHz), X-band communication (8 - 12 GHz), and Ku-band communication (12 - 18 GHz).

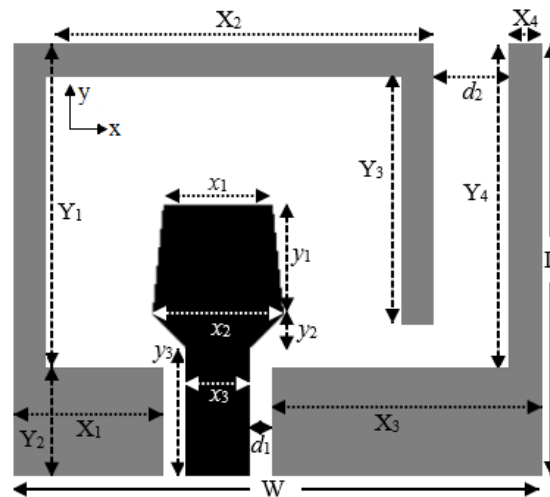


Fig. 1. Schematic diagram of the proposed antenna.

2. Antenna design and analysis

The diagram of the proposed uniplanar antenna is portrayed in Fig. 1. The layout is built on one side of substrate material consists of an epoxy matrix reinforced woven glass. The fiberglass in the composition is 60% while the epoxy resin contributes 40% of the composition which varies in thickness and direction-dependent. The attractive characteristic of epoxy resin composite is that it can be shaped and redesigned frequently without losing its material properties [21]. The main radiator of the proposed antenna is a modified bow-tie-shaped patch with a materialization of copper of thickness 0.035 mm. The bow-tie-shaped patch has two wings of differing sizes and is supported by a CPW line of width x_3 . The length and width of the top wing of the patch are respectively y_1 and x_1 while the tapered transitional wing has the length and width of y_2 and x_2 respectively. The total length of the bow-tie patch is $y_1 + y_2$ and its lower end is connected to the feedline of length y_3 .

To act as a vital source of radiation and to enhance the impedance matching, two coplanar ground planes are placed on $-x$ and $+x$ sides of the radiator. One inverted L-shaped ground plane having a total length of $Y_4 + X_3$ is etched on the right-hand side while an extended U-shaped ground plane having a length of $X_1 + Y_1 + X_2 + Y_3$ is added to the left-hand side of the patch. The inverted L-shaped plane is comprised of two sections of dimension $X_4 \times Y_4$ and $X_3 \times Y_2$. The extended U-shaped plane consists of four sections of size $X_1 \times Y_2$, $X_4 \times Y_1$, $X_2 \times X_4$, and $X_4 \times Y_3$. The space between the feeding line and ground planes is d_1 . The final parameters of the antenna having a dimension of $W \times L$ are $X_1 = 7$ mm, $X_2 = 18$ mm, $X_3 = 12.5$ mm, $Y_1 = 15$ mm, $Y_2 = 5$ mm, $Y_3 = 11.5$ mm, $Y_4 = 15$ mm, $x_1 = 5$ mm, $x_2 = 6$ mm, $x_3 = 3$ mm, $y_1 = 5$ mm, $y_2 = 1.5$ mm, $y_3 = 6$ mm, $d_1 = 1$ mm, $d_2 = 3.5$ mm, $W = 24.5$ mm, and $L = 20$ mm.

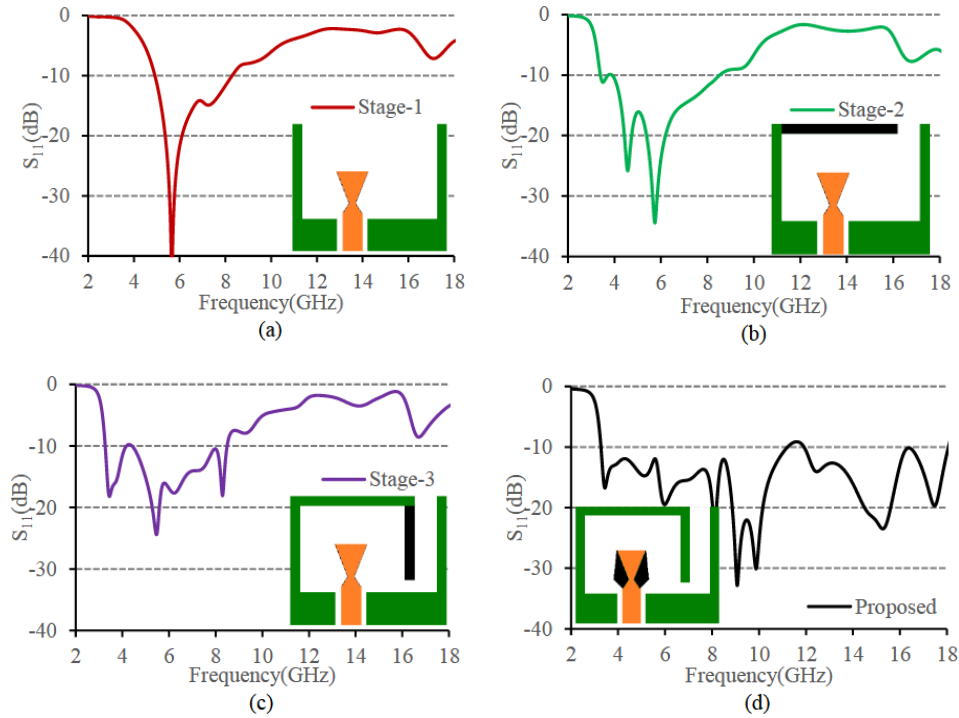


Fig. 2. Simulated S_{11} for different stages of evolution process.

2.1. Design evolution

To understand the operation mechanism, the evolution process of the proposed antenna is displayed in Fig. 2. The S_{11} and input impedance of the different evolution stages are portrayed in Fig. 2. Clearly, it is seen in Fig. 2(a) that the CPW-fed bow-tie-shaped patch with L-shaped and inverted L-shaped ground planes (Stage 1) has a single resonance mode at around 5.66 GHz. In this stage, the antenna achieved an operating band of 4.59 to 8.49 GHz where the input impedance is about 50 ohms. The addition of a horizontal rectangular bar at the upper side of the L-shape ground plane (Stage 2) raises the inductive effect which helps the antenna to exhibit two extra resonant modes at around 3.51 GHz and 4.57 GHz. Consequently, as in Fig 2(b), the antenna in stage 2 achieved dual operating bands of 3.39 - 3.74 GHz and 3.89 - 8.53 GHz where the impedance matching is better than that of stage 1. When another vertical bar of size $X_4 \times Y_3$ is integrated with the L-shaped ground to make it an improved inverted U-shaped ground (Stage 3) as in Fig. 2(c), the second and third resonances move towards the higher operating band due to the increased capacitive effect between L-shaped and U-shaped ground planes. As shown in Fig. 2(c), the operating bandwidth of the first and second bands are respectively 920 MHz (3.26 - 4.18 GHz) and 4.08 GHz (4.41 - 8.49 GHz) where impedances are very much close to 50 ohms. The achieved operating bands of stage 3 are sufficient to cover 4G LTE, 5G sub-6 GHz, WiMAX, WLAN, and UWB communication services but fail to operate at the X-, and Ku-bands. When two arrowhead-shaped portions are appended to the right and left sides of the bow-tie-shaped patch to make an altered bow-tie-shaped patch (Stage 4, the proposed antenna), the impedance matching at higher bands of 8.49 - 11.18 GHz and 11.94 - 18 GHz is drastically improved. As presented in Fig. 2(d), in the lower band, the proposed antenna (Stage 4) exhibits six resonances at around 3.44 GHz, 5.12 GHz, 5.98 GHz, 8.11 GHz, 9.07 GHz, and 9.88 GHz while in the higher band it demonstrates three resonant modes at around 12.46 GHz, 15.27 GHz, and 17.47 GHz. The merging of the first six resonances helps the suggested antenna to attain a working band ranging from 3.28 - 11.21 GHz while the amalgamation of the last three resonances forms a working band of 11.92 to more than 18.0 GHz, and the antenna can cover 4G LTE, 5G sub-6 GHz, WiMAX, WLAN, UWB, X-band and Ku-band wireless communication bands. From the evolution, it is evident that the lower resonant modes are mainly excited by coplanar ground planes whereas the higher resonant modes are excited by the CPW-fed vertical monopole radiator [22].

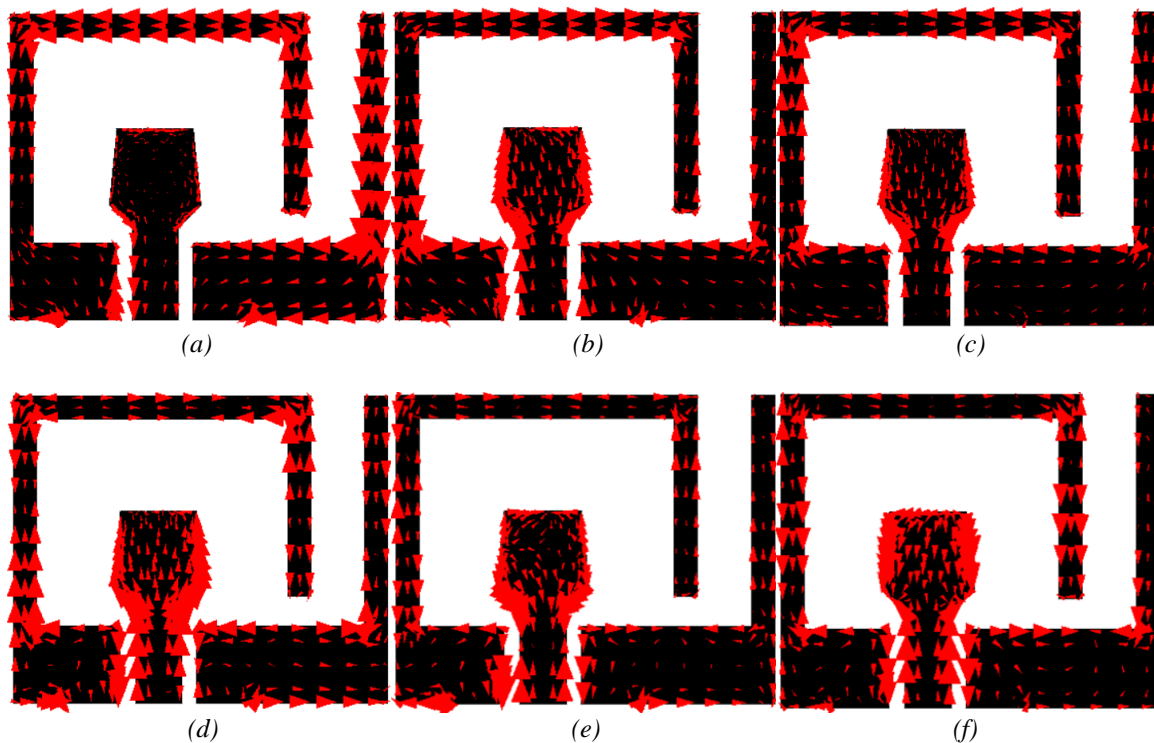


Fig. 3. Vector surface current distributions at (a) 3.44 GHz, (b) 5.12 GHz, (c) 8.11 GHz, (d) 9.88 GHz, (e) 15.27 GHz, and (e) 17.47 GHz.

2.2. Current distribution

As the radiation characteristics of an antenna are reliant on the current density of the antenna surface, the two-dimensional current distribution of the proposed antenna surface is portrayed in Fig. 3. In the plot, the arrow signs specify the current direction. Fig. 3(a) displayed the current distribution at the first resonance frequency of 3.44 GHz. It can be observed that the current density is very high at the inverted L-shaped ground which causes the resonance to occur, and also on the upper portions of the extended inverted U-shaped ground. At this frequency, a negligible amount of current is flowing on the vertical radiator. The current distribution at the second resonance frequency of 5.12 GHz is plotted in Fig. 3(b). As seen in the plot, the current on the inverted L-shaped ground is decreased while the current on the left vertical arm of the inverted U-shaped ground is increased. The concentration of current in the vertical radiator is also remarkably increased. The current distribution at 8.11 GHz is displayed in Fig. 3(c). As seen in Figure, the current concentration at the left vertical arm of inverted U-shaped ground and the vertical radiator is higher than other parts of the antenna. As seen in Fig. 3(d), at 9.88 GHz the current is highly concentrated on the CPW-fed bow-tie-shaped radiator which excites the resonance at this frequency as demonstrates in Figure 2a. The current distribution of the designed antenna at the higher frequencies of 15.27 GHz and 17.47 GHz are respectively demonstrated in Figs. 3(e) and 3(f). It is evident from the figures that the currents on the ground planes are weaker and the currents on the vertical radiator are remarkably higher which confirms that the higher resonance modes are generated by the CPW-fed vertical bow-tie-shaped radiator. As can be observed from the current distribution at each frequency in Fig. 3, lower frequencies have higher current concentrations on coplanar ground planes, while higher frequencies have higher current concentrations on the CPW-fed radiator, supporting the findings in Fig. 2.

3. Results and discussion

To validate the simulated results, the antenna is fabricated with optimized parameters and its photograph is displayed in Fig. 4(a). For signal transmission, a 50-ohm SMA connector is connected to the antenna. The measured scattering parameter (S_{11}) is compared with the simulated one and is shown in Fig. 4(b). An excellent match between simulated and measured outcomes has been accomplished which ensures the suitability of the proposed antenna for WiMAX, WLAN, UWB, X-band, and Ku-band communication. The slight disagreement is primarily on account of fabrication tolerances, SMA soldering effects, and measurement errors. From the measurement, it is evident that the antenna achieved dual operating bands ($S_{11} \leq -10$ dB) of 3.32 - 10.9 GHz (106.6%), and 11.88 - 17.77 GHz (39.7%) that are very much close to the simulation results.

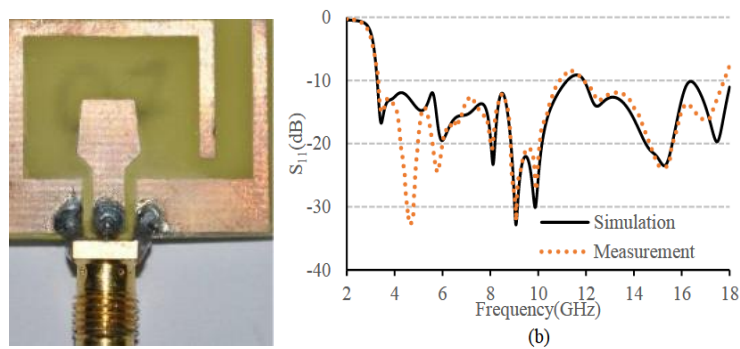


Fig. 4. (a) Prototype, and (b) S_{11} of the proposed antenna.

In order to comprehend the effectiveness of the suggested antenna over the dual operating bands, the radiation characteristics such as gain, efficiency, and radiation patterns are measured using StarLab, the ultimate tool for antenna pattern measurements. The StarLab has a measurement capability from 650 MHz to 18 GHz and the measurement setup is presented in Fig. 5. The simulated and measured peak gain curves of the antenna are illustrated in Fig. 6(a). As observed in the plot, the simulated and measured gain curves are overlapping. In the first band, the studied antenna shows a gain that varies from 0.82 dBi to 4.41 dBi, and the average gain is 3.31 dBi while in the second band the average gain is 6.01 dBi which is varied from 4.68 dBi to 7.01 dBi. In the measured gain curve, a deep has been observed at around 8.9 GHz, which is mainly due to the measurement constraints. The radiation efficiency of the antenna is portrayed in Fig. 6(b). As seen in the graph, in the first band the average measured efficiency is 75.42% and in the second band, it is 83.83% which indicated that most of the power supplied to the antenna is radiated with low loss. The maximum efficiency at the first and second bands are respectively 94.66% and 90.87%.

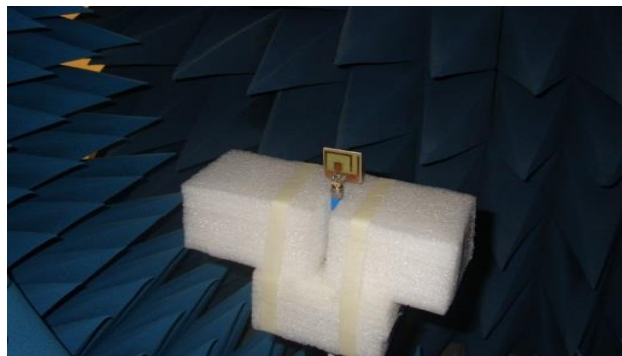


Fig. 5. Radiation characteristics measurement setup in StarLab.

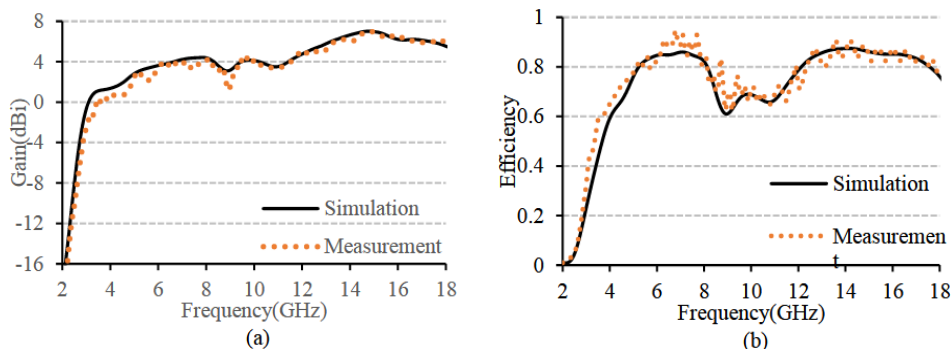


Fig. 6. (a) Gain, and (b) efficiency of the proposed antenna.

The radiation patterns of the proposed antenna for E (yz -plane) and H (xz -plane) planes at 3.44 GHz, 5.12 GHz, 8.11 GHz, and 15.27 GHz are plotted in Fig. 7. From the figure, it is seen that the antenna exhibits an almost omnidirectional radiation pattern. Despite an asymmetrical geometry, the antenna shows symmetrical radiation patterns over the operating bands. At the lower frequency, the cross-polarization component in H -plane is quite higher which may be due to the degenerative effect of the small antennas [23 - 24]. As the ratio of the width and height of the small antennas increases, the larger surface wave produces diffraction at the edge of the dielectric substrate resulting in the production of a higher cross-polarization component [25 - 27]. However, the cross-polarization component decreases with increasing frequency which is due to the increasing antenna size with respect to the corresponding wavelength.

To ensure the UWB operation, the time-domain behavior of the designed antenna has been analyzed. Excellent time-domain characteristics are a prerequisite of UWB antennas. To analyze the time-domain characteristics, two identical antennas are required of which one acts as a transmitter and one acts as a receiver. To calculate the time-domain characteristics, the transmitting antenna and receiving antenna are placed in face-to-face orientation at a distance of 250 mm. The time taken by the antenna to receive the signal is known as group delay that shows the delay of a signal at various frequencies [28]. For distortion-free transmission of a signal, the group delay in the operating band should be linear or flat. The group delay of the suggested antenna in the face-to-face orientation is presented in Fig. 8(a) where its peak-to-peak deviation is lower than 0.75 ns over the two operating bands. This small variation in group delay guarantees that signals are transmitted and received with minimal distortion. The fidelity factor (FF) is another important factor in time-domain analysis that helps to represent the match between the input and received signals [29 - 30]. To calculate the fidelity factor, the input Gaussian pulse is fed to the antenna and the virtual probes are used at the far-field region to receive the transmitted signal. Virtual probes are kept at angles of 0° , 10° , 20° , 30° , 40° , 50° , 60° , 70° , 80° , and 90° at a distance of 250 mm. Fig. 8(b) illustrates the input and output signals in face-to-face arrangement from where it is noticed that the suggested antenna achieved a fidelity factor of 84.04%. As was stated in [28], a fidelity factor of more than 50% is an acceptable value, so the proposed antenna is very much capable of being used in UWB/SWB communication applications. Fig. 8(c) displayed the transfer function (S_{21}) for a pair of proposed antennas. Fairly smooth magnitudes of the transfer function have been observed in the operating bands with some fluctuations in the stopband. The fluctuations in the observed result can be credited to the noise level in the measuring environment. The phase of S_{21} is displayed in Fig. 8(d). A linear phase variation has been observed across the operating bands that ensure that the presented antenna does not introduce any distortion in the phase of the transmitted signal.

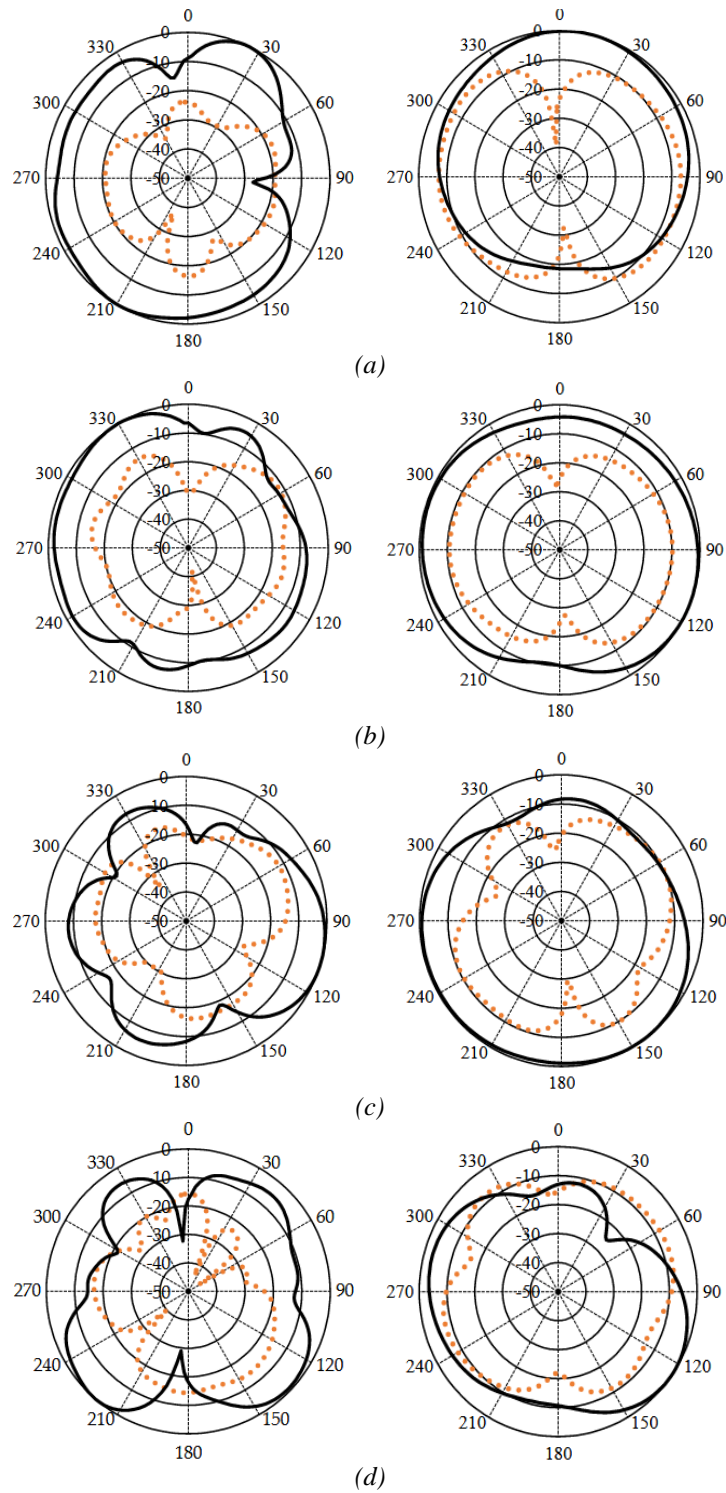


Fig. 7. Measured E-plane(left) and H-plane(right) at (a) 3.44, (b) 5.12, (c) 8.11, and (d) 15.27 GHz. In the plot, the solid and dotted lines are respectively represent the co-polarized and cross-polarized component.

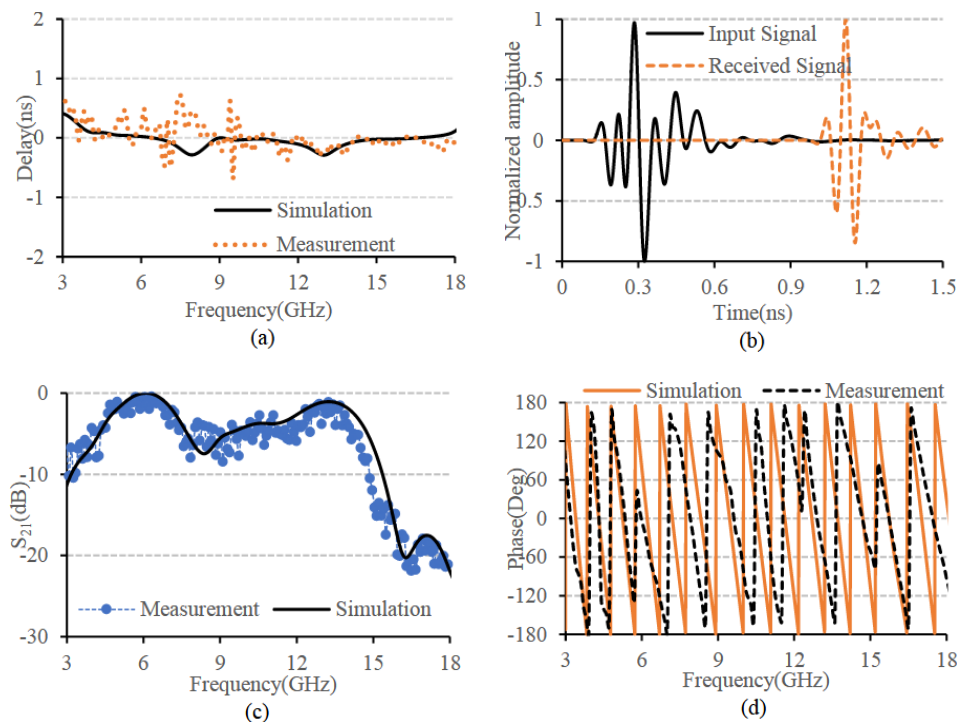


Fig. 8. (a) Group delay, (b) normalized input and received signals, (c) S_{21} , and (d) phase of S_{21} of the proposed antenna.

Table 1. An analysis of recent antenna reports used to compare the proposed antenna performance.

Ref.	Physical size $W_{\text{Sub}} \times L_{\text{Sub}}$	Footprint (mm^2)	Electrical dimension	Operating band(GHz)	BW (GHz)	Gain (dBi)	ϵ_r
[4]	110×120	13200	1.10 λ ×1.20 λ	2.99–10	7.01	6	3.66
[5]	106×85	9010	0.39 λ ×0.31 λ	1.1–11	9.9	5	NR
[6]	75×75	5625	0.74 λ ×0.74 λ	2.94–10.06	6.66	7.5	NR
[7]	80×70	5600	0.99 λ ×0.86 λ	3.7–10.3	6.6	≈ 4.53	2.7
[8]	50×50	2500	0.35 λ ×0.35 λ	2.1–12.6*	10.5	6.88*	4.5
[9]	40×53.3	2132	0.40 λ ×0.53 λ	3.0–18	15	0.7~6.1*	3.58
[10]	42×50	2100	0.39 λ ×0.46 λ	2.78–9.78	7	3.5~6.7	4.7
[11]	40×50	2000	0.47 λ ×0.58 λ	3.5–10.6	7.1	-0.8~4.2	3.55
[12]	41×48	1968	0.41 λ ×0.48 λ	3–15.1	12.1	5.1~8.2	4.4
[13]	35×54	1890	0.26 λ ×0.38 λ	2.1–13.5	11.4	3.9	4.4
[14]	57×32	1824	0.61 λ ×0.34 λ	3.2–13.2	10	2~10	4.4
[15]	55×30	1650	0.63 λ ×0.34 λ	3.43–9.14	5.71	3.92~7.32*	2.33
[16]	39×40	1560	0.34 λ ×0.35 λ	2.6–12.3	9.7	1.98~5.52	4.6
[17]	42×36	1512	0.63 λ ×0.54 λ	4.5–13.5	9	1.9~6.08*	4.4
[18]	24×35	840	0.25 λ ×0.36 λ	3.1–12.3	9.2	2.2~6.8	4.4
[19]	25×30	750	0.24 λ ×0.29 λ	2.9–11.8	8.9	2~6	4.4
[20]	20×29	580	0.21 λ ×0.31 λ	3.15–10.55	7.4	3.9~5.7	2.2
Proposed	24.5×20	490	0.27 λ ×0.22 λ	3.32–10.90 11.88–17.77	7.58 5.89	331 6.01	4.6

*Simulated result, NR-Not reported

In Table 1, the proposed CPW-fed antenna is compared with other wide/ultra-wide/super-wideband antennas that are recently reported. It is clear that the projected antenna has a smaller physical and electrical size than the ones introduced in references [4] to [20]. Though the operating bandwidth of some reported antennas is higher than the proposed one, the antenna presented in this study achieved sufficient bandwidth to cover WiFi, WiMAX, WLAN, UWB, X-, and Ku-communication systems. From the comparison presented in Table 1, it can be commented that the studied antenna guarantees a sensible trade-off between operating band and size.

4. Conclusion

A compact dual-band antenna with an electrical size of $0.27\lambda \times 0.22\lambda$ is presented in this work. To achieve dual-band operation, a CPW-fed modified bow-tie-shaped patch, one inverted L-shaped, and one extended inverted U-shaped ground plane are etched on both sides of epoxy reinforced woven glass material. It is observed that the dual impedance bands are successfully generated employing an adapted bow-tie-shaped radiator along with two coplanar ground planes. The measured findings confirmed that the antenna attains the operating bandwidth of 106.6%, and 39.7% for the first, and second bands respectively with good gain and efficiency. The proposed antenna has numerous advantages such as simple structure, uniplanar profile, compact size, ultra-wideband, and wideband operation, omnidirectional radiation properties, and good time-domain characteristics. Due to the above-mentioned benefits, the designed antenna is an outstanding radiating element for being used in WiMAX, WLAN, UWB, X-band, and Ku-band communication systems.

Acknowledgments

The Deanship of Scientific Research (DSR) at King Abdulaziz University, Jeddah, Saudi Arabia has funded this project, under grant no. (KEP-26-135-42).

References

- [1] M. Samsuzzaman, M. T. Islam, *Microw Opt Technol Lett.* **57**(2), 445(2015).
- [2] P. Okas, A. Sharma, G. Das, R. K. Gangwar, *Int J Electron Commun.* **88**, 63 (2018).
- [3] R. Cicchetti, E. Miozzi, O. Testa, *Int J Antennas Propag.* **2017**, 1 (2017).
- [4] L. Y. Nie, X. Q. Lin, Z. Q. Yang, J. Zhang, B. Wang, *IEEE Trans Antennas Propag.* **67**(4), 2735 (2019).
- [5] H. Nazli, E. Bicak, B. Turetken, M. Sezgin, *IEEE Antennas Wireless Propag Lett.* **9**, 264 (2010).
- [6] Y. Pan, Y. Dong, *IEEE Access* **7**, 160696 (2019).
- [7] R. B. V. B. Simorangkir, A. Kiourti, K. P. Esselle, *IEEE Antennas Wireless Propag Lett.* **17**(3), 493 (2018).
- [8] A. J. A. Al-Gburi, I. M. Ibrahim, Z. Zakaria, M. Y. Zeain, H. Alwareth, A. M. Ibrahim, H. H. Keriee, *Prz Elektrotech* **5**, 70 (2021).
- [9] T. M. Telsang, A. B. Kakade, *Microw Opt Technol Lett.* **56**(2), 362 (2014).
- [10] J. Liang, C. C. Chiau, X. Chen, C. G. Parini, *IEEE Trans Antenna Propag.* **53**(11), 3500 (2005).
- [11] A. A. Omar, O. A. Safia, M. Nedil, *Int J RF Microw Comput Aided Eng.* **27**(7), 1 (2017).
- [12] J. Wu, Z. Zhao, Z. Nie, Q-H. Liu, *IEEE Antennas Wireless Propag Lett.* **13**, 698 (2014).
- [13] R. Kumar, R. Sinha, A. Choubey, S. K. Mahto, *J Electromagn Waves Appl.* **35**(2), 233 (2020).
- [14] R. Kumar, R. K. Khokle, R. V. S. R. Krishna, *IEEE Trans Antennas Propag.* **62**(7), 3501 (2014).
- [15] D. S. Zhang, R. S. Yahya, *Microw Opt Technol Lett.* **59**(10), 2432 (2017).

- [16] R. Azim, M. T. Islam, N. Misran, Arab J Sci Eng. **38**(9), 2415 (2013).
- [17] A. Sharma, P. Khanna, K. Shingha, A. Kumar, J Elec & Computer Eng. **2016**, 1 (2016).
- [18] M. J. Hossain, M. R. I. Faruque, M. M. Islam, M. T. Islam, M. A. Rahman, Frequenz **70**(11-12), 473 (2016).
- [19] Y. Yang, Z. Zhao, X. Ding, Z. Nie, Q-H. Liu, IEEE Trans Antennas Propag. **67**(1), 140 (2019).
- [20] S. Zhang, Y. Zhong, Y. Zhou, Y. Guo, C. Ji, IEICE Electron Expr. **16**(20), 1 (2019).
- [21] I. Yarovsky, E. Evans, Polymer, **43**(3), 963 (2002).
- [22] A. T. Mobashsher, M. T. Islam, Meas Sci Rev. **13**(4), 169 (2013).
- [23] R. Azim, M. T. Islam, N. Misran, Telecommun Syst. **52**(2), 1171(2013).
- [24] W.-P. Lin, C.-H. Huang, IEEE Antennas Wirel Propag Lett. **8**, 228 (2009).
- [25] Z.-A. Zheng, Q.-X. Chu, Electron Lett. **45**(12), 593 (2009).
- [26] Y. Q. Xia, Z. G. Duan, Electron Lett. **44**(9), 567 (2008).
- [27] A. T. Mobashsher, M. T. Islam, N. Misran, Appl Comput Electromagn Soc J. **26**(1), 73 (2011).
- [28] G. Quintero, J. F. Zurcher, A. K. Skrivervik, IEEE Trans Antennas Propag. **59**(7), 2502 (2011).
- [29] Q. Wu, R. Jin, J. Geng, M. Ding, IEEE Trans Antennas Propag. **55**(10), 2866 (2007).
- [30] M. M. Alam, R. Azim, I. M. Mehedi, A. I. Khan, Chin J Phys. **73**, 684(2021).